SAND2016-6422J

Scaling effects in sodium zirconium silicate phosphate ($Na_{1+x}Zr_2Si_xP_{3-x}O_{12}$) ion conducting thin films

Jon F. Ihlefeld[1, a), *] Emily Gurniak,[1] Brad H. Jones,[1] David R. Wheeler,[1] Mark A. Rodriguez,[1] and Anthony H. McDaniel[2, *]

[1]*Sandia National Laboratories, Albuquerque, New Mexico 87185, USA*
[2]*Sandia National Laboratories, Livermore, California, 94551 USA*

Abstract:
Preparation of sodium zirconium silicate phosphate (NaSICon), $Na_{1+x}Zr_2Si_xP_{3-x}O_{12}$ ($0.25 \leq x \leq 1.0$), thin films has been investigated via a chemical solution approach on platinized silicon substrates. Increasing the silicon content resulted in a reduction of the crystallite size and a reduction in the measured ionic conductivity. Processing temperature was also found to affect microstructure and ionic conductivity with higher processing temperatures resulting in larger crystallite sizes and higher ionic conductivities. The highest room temperature sodium ion conductivity was measured for an x=0.25 composition at 2.3×10^{-5} S/cm. The decreasing ionic conductivity trends with increasing silicon content and decreasing processing temperature are consistent with grain boundary and defect scattering of conducting ions.

a) Electronic mail: jihlefe@sandia.gov
* Member, The American Ceramic Society

1. Introduction:

Solid-state ion-conducting thin films are of interest for small-scale and mobile energy storage applications. The use of solid-state ion conductors as separators in ion battery chemistries is advantageous under consideration of safety and packaging requirements.[1] For example, in lithium ion batteries solid inorganic ion conductors can be inherently more robust against dendrite formation,[2] which can pierce polymer membranes leading to short circuits and potential for combustion of liquid electrolytes. Existing solid-state thin film battery technologies rely primarily on configurations with lithium phosphorus oxynitride (LiPON) ion conductors. The ease of preparation by physical vapor approaches, ability to deposit films at room temperature, and electrochemical stability over a broad voltage range makes LiPON an attractive option. LiPON, however, is hindered by a relatively low lithium ion conductivity (~2.3×10^{-6} S/cm at 25 °C),[3] which can impart a large internal resistance to the battery and limit usage in applications requiring high power performance. This limitation has led to investigations of alternative separator materials with higher ionic conductivities.[4-6] Processing and electrochemical stability challenges of these alternative ion conductors have limited their deployment.

To circumvent these challenges, research into sodium ion batteries has been undertaken. Here, the existence of super ionic conductors such as β-Al_2O_3 and $Na_{1+x}Zr_2Si_xP_{3-x}O_{12}$ (sodium super ionic conductor, or NaSICon) presents an opportunity for the preparation of high power solid-state batteries. To be applicable for thin film batteries, however, preparation methods of these materials must be demonstrated. We have previously shown that the phosphate end member of NaSICon, $NaZr_2P_3O_{12}$, can be prepared via a chemical solution deposition approach using an alkoxide-based chemistry.[7] We demonstrated that preparation on platinized silicon substrates results in preferentially (012)-textured films with room temperature ionic conductivities as high as 5×10^{-7} S/cm. This value is 2 times higher than has been reported for bulk materials of the same composition,[8] which we attribute to increased density – the bulk ceramics were reported to be 85-90% dense – in the thin film samples. This high ion conductivity with respect to bulk ceramic counterparts notwithstanding, this value remains low compared to other thin film ion conductors, such as LiPON.

A means to increase the ionic conductivity of NaSICon is to substitute silicon (and an additional sodium for charge balance) for phosphorus.[9] By replacing phosphorus with silicon, the size of the lattice openings through which sodium must travel are increased, leading to increasing ionic conductivity with increasing silicon content. Room temperature ionic conductivities of 6×10^{-4} S/cm are possible for compositions substituting two silicon for phosphorus (x=2),[10] which is the composition of peak ionic conductivity in NaSICon.[9] Compositions containing silicon in excess of x=2 result in a decrease in ionic conductivity owing to a decrease in the size of the lattice openings for sodium transport. While these trends have been widely demonstrated in bulk materials,[11] reports on the preparation of silicon-containing NaSICon films are limited.[12-16] In many of the reports that do exist it is not readily evident that phase-pure NaSICon films have been successfully prepared. In this work we present our efforts to incorporate silicon into NaSICon thin films prepared via chemical solution deposition on platinized silicon substrates. We will show that small amounts of silicon (x=0.25) can be incorporated with significant increases in the ionic conductivity, but that further increases in the silicon content do not result in commensurate increases in ionic conductivity. This diminished (and decreasing) ionic conductivity for silicon levels >0.25 is attributed to decreased crystallite and grain size, resulting in an increased number of grain boundaries and possibly defective crystallites for the given thermal constraints imposed by the substrates.

Experimental Procedure:

An alkoxide-based chemistry similar to that used in our prior research[7] on $NaZr_2P_3O_{12}$ and based upon that outlined by Gasmi, *et al.*[17] and Martucci *et al.*[18] was used for solution preparation. Precursor chemicals used include: sodium ethoxide (≥95%, Fluka, Sigma-Aldrich), zirconium butoxide (80 wt% in butanol, Sigma-Aldrich), tetraethylorthosilicate (TEOS, 99.99%, Sigma-Aldrich), dibutyl phosphate (≥97%, Sigma-Aldrich), and 1-butanol (99.8%, Sigma-Aldrich). 12 mL total volume, 0.15 M, as referenced to an entire formula unit, solutions were prepared. The synthesis procedure was as follows: the desired mass of zirconium butoxide (1.7266 g) was weighed into a vial, 1-butanol (~9.3 – 9.2 mL for x=0.25 to x=1, respectively), TEOS (0.0937 – 0.3750 g for x=0.25 to x=1, respectively), dibutyl phosphate (1.041 - 0.7568 g for x=0.25 to x=1,

respectively), and sodium ethoxide (0.1531 - 0.2450 g for x=0.25 to x=1, respectively) were sequentially added with ~30 minute – 1 hour stirring between steps. Solution synthesis was conducted within an argon-filled glove box to minimize exposure to moisture and oxygen. Films were spin cast in laboratory ambient conditions onto $Pt/TiO_x/SiO_2/Si$ substrates (nominal layer thicknesses of 100 nm/40 nm/400 nm/handle, respectively) that were prepared in-house by RF magnetron sputtering. The substrate preparation sequence involved the deposition of titanium metal onto the SiO_2/Si wafer (SiliconQuest International, Santa Clara, CA). The wafer was then removed from vacuum and annealed at 400 °C for 10 minutes in air in a preheated box furnace. The platinum layer was then deposited and the wafer annealed at 700 °C in air for 10 minutes. The solutions were spin cast at 3000 RPM onto diced sections of the platinized silicon wafer, pyrolyzed on a hotplate at 300 °C for 5 minutes, and then directly inserted into a preheated tube furnace for crystallization for 10 minutes. The crystallization anneal was conducted at temperatures of 750, 775, or 800 °C. The process was repeated two times such that three total layers (approximately 300 nm of as-crystallized film, verified by cross-sectional scanning electron microscopy) were deposited. Platinum contacts ~500 μm × 500 μm defined by a shadow mask and ~90 nm thick were deposited to the top of the film to form metal-electrolyte-metal structures for impedance measurements. Electrode areas were measured via optical microscopy. All impedance measurements were conducted with a HP4192A (Keysight Technologies, Santa Rosa, CA) instrument over a range of 1 MHz to 5.7 Hz using a 50 mV (rms) oscillator. Fits to the complex plane impedance data were made using Bio-Logic EC-Lab software (version 10.32, Bio-Logic, Claix, France). Temperature dependent measurements were made on samples adhered to alumina coupons (CoorsTek, Golden, CO) with gold wire bonds (California Fine Wire, Grover Beach, CA) applied to the surfaces of the platinum electrodes using silver epoxy (Epo-Tek H20E, Epoxy Technology, Billerica, MA). The gold wire bonds led to 24 gauge wires, which were connected to contacts within a Delta Design 9023 (Cohu SEG, San Diego, CA) chamber. Film phase assemblage was studied using X-ray diffraction (XRD) with Cu Kα radiation (Phaser X2, Bruker, Madison, WI). Profile fitting of XRD data for crystallite size determination was performed using Jade (version 9.6, Materials Data, Inc., Livermore, CA). A Pearson-VII profile shape was used to

model the peak shape and determine the full width at half maximum (FWHM) for the desired reflection. Crystallite size values were estimated based on the reflection FWHM using Scherrer's equation[19] after accounting for instrument broadening via a known standard (NIST SRM 1976 Alumina plate, National Institute of Standards and Technology, Gaithersburg, MD). Errors are the estimated standard deviations provided by the Jade software. Film microstructure was studied with scanning electron microscopy (SEM) in an in-lens imaging mode with a Zeiss Supra 55VP instrument (Jena, Germany). A thin layer of 60-40 Au-Pd was deposited on the samples prior to imaging to minimize charging effects.

Results and Discussion:

Figure 1 shows representative XRD patterns for films with crystallization anneal temperatures of 750, 775, and 800 °C and compositions of $Na_{1+x}Zr_2Si_xP_{3-x}O_{12}$ (a) x=0.25, (b) x=0.5, (c) x=0.75, and (d) x=1.0. Bar markers indicating the expected peak positions of rhombohedral $NaZr_2P_3O_{12}$[20] (NZP) and tetragonal-ZrO_2[21] are inserted in the plots. Note that all of these compositions are expected to be of the rhombohedral phase,[9, 20] thus motivating the selection of the NZP end-member for indexing purposes of the peaks in Figure 1, while the actual peaks may shift slightly owing to solid solution and strain effects. ZrO_2 is a commonly observed impurity in NaSICon powders,[22] ceramics,[23-25] and films[14] and a broad peak consistent with tetragonal ZrO_2 is observed at ~30.2° in 2θ. The intensity of the ZrO_2 secondary phase appears to scale with increasing silicon content as it is hardly noticeable in the x=0.25 composition and becomes more prevalent in the x=0.75 and x=1 compositions.

For the x=0.25 composition, strong (012) crystallographic texture is observed, which is similar to that identified for the x=0 composition in prior work.[7] As the crystallization anneal temperature is increased, the NaSICon X-ray peaks begin to narrow and intensify, indicating an increase in crystallinity. With increasing silicon in the NaSICon composition from x=0.25 to x=1, the strong crystallographic texture diminishes and the 012 peaks are barely apparent for the x=0.75 and x=1 compositions. The most intense peaks observed for the x=0.5, 0.75, and 1 compositions are 110 and 113, which correspond to the most intense reflections in a powder sample, and indicate that these

films possess increasingly random grain orientations. In addition to a reduction in the degree of crystallographic texture, the reflection widths increase with increasing silicon content for each given temperature, which is indicative of smaller crystallite sizes. Crystallite size was assessed using the 113 reflection using the method discussed in the experimental procedure. The 113 peak was chosen as it is present in each film and is the most intense peak in NaSICon powders and is reasonably separated from other reflections to enable unambiguous peak width measurement.[26] As shown in Figure 2, a general trend of decreasing crystal coherence length with increasing silicon content is observed. The x=0.25 composition has larger crystallite sizes for each process temperature than higher silicon content films. Also, as the processing temperature is increased the crystallite size appears to increase for each film, which is consistent with increased mass transport at higher temperatures resulting in larger crystallites. The change in crystallographic texture and reduction of crystallite size with increasing silicon content suggests a change in nucleation and growth mechanism in these films. Strong crystallographic textures are typically observed in thin film samples that nucleate heterogeneously at interfaces – usually when some degree of lattice matching is present. For these films, however, no obvious lattice match of the NaSICon (012) planes to the platinum (111) planes could be found. Regardless, the degree of texture changes significantly with increasing silicon content. Homogeneous nucleation within the thickness of the film with increasing populations of NaSICon nuclei could result in the reduced crystallite size in higher silicon content films. It is further possible that the silicon-containing films are more refractory than the lower silicon content films, resulting in limited grain growth, which is supported by the decreasing magnitude of crystallite size increase with processing temperature as the silicon content increases. Note that the x=0.25 composition does show a maximum in crystallite size for a 775 °C anneal rather than the 800 °C condition. This may result from an increase in (012) texture for the 800 °C processed sample resulting in fewer and smaller (113) oriented grains, which would lead to increased 113 peak breadth. Indeed, the 012 peak is 6 times more intense than the 113 peak for the 800 °C processed sample and only 2 times more intense for the 775 °C processed sample, which is consistent with improved degree of texture for the 800 °C processed sample.

Figure 3 shows representative plan-view scanning electron micrographs for films processed with 800 °C crystallization anneals. Consistent with the crystallite size derived from X-ray scattering, a decreasing feature size is observed as the silicon content is increased. Statistically relevant measurement of physical grain size from SEM micrographs was only possible for the x=0.25 composition where discrete grain boundaries could be observed. Average grain sizes were assessed using a linear intercept method[27] for this composition and were found to be 52 ± 4.9, 53 ± 4.5, and 60 ± 6.1 nm for processing temperatures of 750, 775, and 800 °C, respectively. These values are larger than the crystalline coherence length measured from X-ray scattering, which is a typical trend for ceramic thin films, where sub-grain defects can result in crystallite sizes smaller than the average physical grain size.[28, 29] For the x=0.25 composition, fine grains that appear as brighter features are observed at grain boundaries. Similarly sized features are observed on the surfaces of the other films. The increased brightness of the features is consistent with a higher average atomic number. Given the fine size and brightness of these features, we believe that these are the tetragonal ZrO_2 phases that are observed in the XRD data, as discussed in prior work.[7] Plan-view SEM images for 750 and 775 °C processed films are shown in supplemental information in Figures S1 and S2, respectively. Fracture cross-section SEM images for 775 °C processed films of all compositions are shown in Figure S3. Granular features in these cross-sections possess decreasing dimensions as the silicon content is increased, which is consistent with the crystalline coherence length measurements. Similar to the plan-view grain sizes measured for the x=0.25 composition, these grains appear to be slightly larger than the measured crystalline coherence length.

Representative room temperature complex plane impedance plots are shown in Figure 4 for the 800 °C annealed samples for each composition. The complex-plane impedance response comprises a high-frequency arc and a low frequency spike of increasing absolute imaginary impedance. This signature is consistent with ion conduction within an electrolyte (arc) and ionically blocking electrodes (spike).[30] The data were fit with a ZARC (resistor and constant phase element in parallel) in series with a constant phase element. These fitting elements are commonly used for solid electrolytes where slightly depressed arcs rather than perfect semicircles exist.[31] High quality fits,

with χ^2 values less than 1 Ohm, are achieved in each case. Using the resistance calculated from the ZARC element with the measured film thicknesses and electrode areas, the total ion conductivity could be determined for each composition. Figure 5 compares the room temperature ionic conductivity for each processing temperature and composition and includes prior work on x=0 films.[7] Contrary to the expected trend based on composition in bulk samples, where ionic conductivity increases with increasing silicon content for compositions $0 \leq x \leq 2$,[9, 11] the maximum ion conductivity for films is observed with a x=0.25 composition with a value of 2.3×10^{-5} S/cm for the 800 °C processed sample. While this conductivity is substantially higher than the x=0 end member composition (5×10^{-7} S/cm),[7] suggesting an opening of the ion conducting channels, we do not observe an increasing ionic conductivity with further increasing silicon content. Rather, within each iso-processing temperature set, compositions containing silicon beyond x=0.25 had decreasing room temperature ion conductivities. Within each iso-composition sample set, an increased ionic conductivity is observed with increasing processing temperature, with a magnitude of increase of ~40× for the x=0.25 composition to ~4.6× for the x=1 composition. We hypothesize that the composition and processing temperature dependency is due to decreasing grain and crystallite size with increasing silicon content. Decreasing crystallite size can result from decreasing grain size and sub-grain defects, such as dislocations, tilt boundaries, and stacking faults. Bulk ceramic NaSICon materials, which display the expected high ionic conductivity with increased silicon content, typically have grain sizes in excess of 1 μm – at least an order of magnitude larger than those in our films.[32, 33] Additionally, bulk ceramics are typically sintered at temperatures in excess of 1100 °C and would be expected to have reduced crystalline mosaicity. Thin films of the x=0 end member had much larger grain sizes (up to 142 nm for 800 °C processed samples) than the samples in this study and also had larger crystallite sizes (larger than 100 nm, which is the resolution limit where instrument broadening dominates for the XRD instrument, for the 012 reflection of the 800 °C processed sample), which may account for the bulk-like performance.[7] It appears that the increased concentration of grain boundaries, and possibly defects, in these thin film samples results in a reduction in the ionic conduction in these films, particularly for the x=0.5, x=0.75, and x=1 compositions where influence of crystallographic texture is

minimal as these films are randomly oriented. For the x=0.25 composition film, it is possible that the increased crystallographic texture, in addition to larger crystallite size, could lead to a higher measured ionic conductivity.[34] However, direction-dependent ion conductivity measurements have been performed on x=0 single crystals, which has the same symmetry as the x=0.25 composition, and no conduction anisotropy was observed,[35] which suggests that crystallographic texture does not contribute to the higher ion conductivity observed in samples of this composition. More likely, the crystallographic texture results in a columnar grain morphology that has decreased numbers of grain boundaries through the film thickness. Cross-sectional SEM images as shown in the supplemental information, Figure S4, reveal a microstructure consistent with this grain morphology.

It is prudent to consider whether the dominant conduction mechanism changes from intragranular to grain boundary or vice versa and understand how this could affect the measured ion conductivities. Two separate ZARC elements, which are employed to fit bulk polycrystalline ion conductors with discrete intragrain and grain boundary responses, did not provide improved fits to the data and we were unable to resolve separate ZARCs, which would directly clarify this possibility (see supplementary Tables SI and SII and Figure S5). However, area and thickness normalized capacitance values could be determined from the ZARCs. For the 800 °C processed samples, normalized capacitance values of 3.9 pF/cm and 13.7 pF/cm were calculated for the x=0.25 and x=1 compositions, respectively. These values are more than an order of magnitude smaller than a normalized capacitance value (250 pF/cm) that has been attributed to grain boundaries in other solid ion conductors.[36] This suggests that the dominant conduction pathway in these films is intragranular.

The presence of the ZrO_2 impurity phase or an amorphous phase not identifiable in the X-ray diffraction patterns also needs to be considered as a contributor to the decreased ionic conductivity. We cannot rule out some role of secondary phases inhibiting ionic conduction, but do note that we did not need to use additional resistors in our models to fit the impedance data. This suggests that the ZrO_2 phase or possible unidentified amorphous phases are not present as discrete layers, but rather as distributed in a NaSICon matrix. Prior studies on the x=0 composition showed that ZrO_2 was present

as fine grains distributed through the thickness of the film[7] and the SEM data of these samples (see Figure S4) supports this. These factors combined, we deduce that the reduced crystallinity with increasing silicon content is the dominant factor in reduced ion conductivity. Limitations in ionic conduction due to grain boundaries or intragranular defects has been identified by prior researchers in many inorganic ion conductors,[37-40] including NaSICon,[33] and our results are consistent with these prior observations.

Temperature dependence of ionic conductivity is shown in an Arrhenius plot in Figure 6 for the 800 °C crystallized samples as measured between room temperature and 150 °C. Consistent with the room temperature measurements, we observe higher ionic conductivities for lower silicon content compositions. Activation energies for ionic conduction were assessed from the slopes of the conductivity versus inverse temperature (note that extrinsic conduction was assumed here and conductivity × absolute temperature was used as the ordinate axis).[41] We calculate values of 0.31, 0.33, 0.40, 0.37 eV for the x=0.25, 0.5, 0.75, and 1 compositions, respectively. These values are comparable to similar composition bulk ceramics (0.26 and 0.31 eV for x=0.4 and 0.8, respectively).[9] These similar values provide additional evidence that the bulk-like ion conduction mechanisms are occurring in these films, but that the reduced ion conduction values are due to an extrinsic source – very fine grain sizes and reduced crystallinity resulting from increasing silicon content.

Finally, while we were unable to realize the extremely high ionic conductivities expected for increasing silicon content (aside from the ~46× increase for the x=0.25 composition compared to the x=0 composition), the role of the substrate must be appreciated. In this work we utilized platinized silicon substrates with a TiO_2 adhesion layer between the platinum layer and the SiO_2/Si substrate. These substrates impose thermo-physical limitations on the maximum processing temperature that can be used (~800 °C). Higher temperatures are known to result in dewetting, hillocking, and delamination of the platinum layer.[42] We explored the processing of these films on Pt/ZnO/SiO_2/Si substrates, which we have previously shown enables access to temperatures of 900 °C without dewetting or delamination.[43] At the same processing temperatures used for films in this study, we observed a secondary phase identified as $NaZnPO_4$[44] that became more prevalent with increasing silicon content (see supplemental

Figure S6). Electron microscopy revealed that the platinum layer was dewetting and exposing the ZnO adhesion layer in these films as shown in supplemental Figure S7. We speculate that the increasing sodium concentration that is necessary for charge balance when substituting silicon for phosphorus is responsible for this behavior. Increased sodium content may result in sodium reacting with the platinum electrode potentially resulting in a lower melting temperature sodium-platinum alloy that dewets at the crystallization temperatures used.[45] This dewetting behavior was not observed using the $Pt/TiO_2/SiO_2/Si$ substrates. We suspect that the finite amount of titanium diffusion that is known to occur into the platinum layer from the TiO_2 adhesion layer may mechanically stabilize the platinum electrode and prevent dewetting under these processing conditions. No secondary phases containing titanium were observed, so we do not believe that titanium diffusion significantly degraded the performance of the NaSICon films. In order to realize the expected high ionic conductivities of silicon-containing NaSICon in a thin film, methods to increase crystallite size may be necessary. It is possible that alternative approaches such as: 1) a solution chemistry that more effectively binds the sodium into a gel network, 2) physical vapor deposition, or 3) an alternative electrode structure may enable such films to be prepared.

Conclusions:

In summary, we have prepared $Na_{1+x}Zr_2Si_xP_{3-x}O_{12}$ thin films in the composition range of x=0.25 to x=1.0 via chemical solution deposition. The following general trends were found:

1) Increasing the silicon content from x=0.25 to x=1.0 resulted in a decrease in crystallographic texture and a decrease in the average crystallite size in the films.
2) Increasing process temperature from 750 to 800 °C resulted in an increase in the average crystallite size for most compositions.
3) The highest room temperature ionic conductivity was observed for the x=0.25 composition processed at 800 °C. Increasing the silicon content and/or decreasing the processing temperature resulted in a decrease in the measured ionic conductivity.

4) The observed trends of decreasing ionic conductivity with increasing silicon content can be correlated with a decrease in crystallite size.

Acknowledgements:

The authors wish to acknowledge experimental assistance from Mia Blea-Kirby and Bonnie B. McKenzie and critical review of this manuscript by Dr. Erik Spoerke. This research was supported by the Laboratory Directed Research and Development program at Sandia National Laboratories, a multi-program laboratory managed and operated by Sandia Corporation, a wholly owned subsidiary of Lockheed Martin Corporation, for the U.S. Department of Energy's National Nuclear Security Administration under contract DE-AC04-94AL85000.

References:

[1]J. G. Kim, B. Son, S. Mukherjee, N. Schuppert, A. Bates, O. Kwon, M. J. Choi, H. Y. Chung, and S. Park, "A review of lithium and non-lithium based solid state batteries," *J. Power Sources,* **282** 299-322 (2015).

[2]E. G. Herbert, W. E. Tenhaeff, N. J. Dudney, and G. M. Pharr, "Mechanical characterization of LiPON films using nanoindentation," *Thin Solid Films,* **520** [1] 413-418 (2011).

[3]X. H. Yu, J. B. Bates, G. E. Jellison, and F. X. Hart, "A stable thin-film lithium electrolyte: Lithium phosphorus oxynitride," *J. Electrochem. Soc.,* **144** [2] 524-532 (1997).

[4]K. Takada, K. Fujimoto, T. Inada, A. Kajiyama, M. Kouguchi, S. Kondo, and M. Watanabe, "Sol–gel preparation of Li+ ion conductive thin film," *Appl. Surf. Sci.,* **189** [3–4] 300-306 (2002).

[5]J. F. Ihlefeld, P. G. Clem, B. L. Doyle, P. G. Kotula, K. R. Fenton, and C. A. Apblett, "Fast Lithium-Ion Conducting Thin-Film Electrolytes Integrated Directly on Flexible Substrates for High-Power Solid-State Batteries," *Adv. Mater.,* **23** [47] 5663 (2011).

[6]C.-L. Li, B. Zhang, and Z.-W. Fu, "Physical and electrochemical characterization of amorphous lithium lanthanum titanate solid electrolyte thin-film fabricated by e-beam evaporation," *Thin Solid Films,* **515** [4] 1886-1892 (2006).

[7]W. Meier, C. Apblett, D. Ingersoll, A. McDaniel, and J. F. Ihlefeld, "Preparation and Processing Temperature Effects on Ion Conductivity in Solution Derived Sodium Zirconium Phosphate ($NaZr_2P_3O_{12}$) Thin Films," *J. Electrochem. Soc.,* **161** [3] A364-A367 (2014).

[8]M. Nagai, S. Fujitsu, and T. Kanazawa, "Ionic-Conductivity in the System $NaZr_2(PO_4)_3$-$Na_3Y_2(PO_4)_3$," *J. Am. Ceram. Soc.,* **63** [7-8] 476-477 (1980).

[9]J. B. Goodenough, H. Y. P. Hong, and J. A. Kafalas, "Fast Na^+-ion transport in skeleton structures," *Mater. Res. Bull.,* **11** [2] 203-220 (1976).

[10]O. Bohnke, S. Ronchetti, and D. Mazza, "Conductivity measurements on nasicon and nasicon-modified materials," *Solid State Ionics,* **122** [1-4] 127-136 (1999).

[11]E. Breval, H. A. McKinstry, and D. K. Agrawal, "Sodium ionic conductivities of substituted NZP materials," *Brit. Ceram. T.,* **93** [6] 239-251 (1994).

[12]Y. L. Huang, A. Caneiro, M. Attari, and P. Fabry, "Preparation of NASICON thin films by dip coating on Si/SiO_2 wafers and corresponding C-V measurements," *Thin Solid Films,* **196** [2] 283-294 (1991).

[13]D. Ivanov, J. Currie, H. Bouchard, A. Lecours, J. Andrian, A. Yelon, and S. Poulin, "Sputtered silicate-limit NASICON thin films for electrochemical sensors," *Solid State Ionics,* **67** [3-4] 295-299 (1994).

[14]Y. Shimizu and T. Ushijima, "Sol-gel processing of NASICON thin film using aqueous complex precursor," *Solid State Ionics,* **132** [1-2] 143-148 (2000).

[15]P. A. Lessing and G. Huestis, "Synthesis of nanocrystalline NASICON-type thin film ceramics," *J. Ceram. Process Res.,* **7** [1] 1-9 (2006).

[16]R. Izquierdo, E. Quenneville, D. Trigylidas, F. Girard, M. Meunier, D. Ivanov, M. Paleologou, and A. Yelon, "Pulsed laser deposition of NASICON thin films for the fabrication of ion selective membranes," *J. Electrochem. Soc.,* **144** [12] L323-L325 (1997).

[17]N. Gasmi, N. Gharbi, H. Zarrouk, P. Barboux, R. Morineau, and J. Livage, "Comparision of Different Synthesis Methods for Nasicon Ceramics," *J. Sol-Gel Sci. Technol.,* **4** [3] 231-237 (1995).

[18]A. Martucci, S. Sartori, M. Guglielmi, M. L. Di Vona, S. Licoccia, and E. Traversa, "NMR and XRD study of the influence of the P precursor in sol-gel synthesis of NASICON powders and films," *J. Eur. Ceram. Soc.,* **22** [12] 1995-2000 (2002).

[19]P. Scherrer, "Estimation of the size and structure of colloidal particles by Röntgen rays," *Nachr. Ges. Wiss. Goettingen, Math.-Phys. Kl.,* **2** 96-100 (1918).

[20]H. Y. P. Hong, "Crystal structures and crystal chemistry in the system $Na_{1+x}Zr_2Si_xP_{3-x}O_{12}$," *Mater. Res. Bull.,* **11** [2] 173-182 (1976).

[21]L. Lutterotti and P. Scardi, "Simultaneous structure and size-strain refinement by the Rietveld method," *J. Appl. Crystallogr.,* **23** [4] 246-252 (1990).

[22]N. S. Bell, C. Edney, J. S. Wheeler, D. Ingersoll, and E. D. Spoerke, "The Influences of Excess Sodium on Low-Temperature NaSICON Synthesis," *J. Am. Ceram. Soc.,* **97** [12] 3744-3748 (2014).

[23]U. Von Alpen, M. F. Bell, and H. H. Hofer, "Compositional Dependence of the Electrochemical and Structural Parameters in the NASICON system ($Na_{1+x}Si_xZr_2P_{3-x}O_{12}$)," *Solid State Ionics,* **3-4** [AUG] 215-218 (1981).

[24]M. L. Bayard and G. G. Barna, "Complex impedance analysis of ionic-conductivity of $Na_{1+x}Zr_2Si_xP_{3-x}O_{12}$ ceramics," *J. Electroanal. Chem.,* **91** [2] 201-209 (1978).

[25]V. A. Nicholas, P. J. Johnson, and A. I. Kingon, "Conductivity measurements in the NASICON system," *Solid State Ionics,* **17** [4] 351-357 (1985).

[26]"Sodium Zirconium Phosphate, Reference code: 00-033-1312," *Natl. Bur. Stand. Monogr.,* **19** [25] 81 (1982).

[27]ASTM E 112-96, "Standard Test Methods for Determining Average Grain Size," **Vol. 03.01**. ASTM International, (2003).

[28]J. F. Ihlefeld, J. C. Ginn, D. J. Shelton, V. Matias, M. A. Rodriguez, P. G. Kotula, J. F. Carroll, G. D. Boreman, P. G. Clem, and M. B. Sinclair, "Crystal coherence length effects on the infrared optical response of MgO thin films," *Appl. Phys. Lett.,* **97** [19] 191913 (2010).

[29]J. F. Ihlefeld, A. M. Vodnick, S. P. Baker, W. J. Borland, and J.-P. Maria, "Extrinsic scaling effects on the dielectric response of ferroelectric thin films," *J. Appl. Phys.,* **103** [7] 074112 (2008).

[30]J. T. S. Irvine, D. C. Sinclair, and A. R. West, "Electroceramics: Characterization by Impedance Spectroscopy," *Adv. Mater.,* **2** [3] 132-138 (1990).

[31]J. R. Macdonald, "Note on the parameterization of the constant-phase admittance element," *Solid State Ionics,* **13** [2] 147-149 (1984).

[32]J. W. Hoj and J. Engell, "Ion conductivity of NASICON ceramics: Effects of texture and doping with B_2O_3 and Al_2O_3," *Mater. Sci. Eng. B-Solid State Mater. Adv. Technol.,* **19** [3] 228-233 (1993).

[33]R. O. Fuentes, F. M. Figueiredo, F. M. B. Marques, and J. I. Franco, "Influence of microstructure on the electrical properties of NASICON materials," *Solid State Ionics,* **140** [1-2] 173-179 (2001).

[34]K. D. Kreuer, H. Kohler, U. Warhus, and H. Schulz, "Nasicon solid electroyltes Part III: Sodium conductivity enhancement along domain and grain boundareis," *Mater. Res. Bull.,* **21** [2] 149-159 (1986).

[35]A. K. Ivanov-Schitz and A. B. Bykov, "Ionic conductivity of the $NaZr_2(PO4)_3$ single crystals," *Solid State Ionics,* **100** [1-2] 153-155 (1997).

[36]Y. Saito, K. Ado, T. Asai, H. Kageyama, and O. Nakamura, "Grain-boundary ionic conductivity in norminal $Li_{1+x}M_xTi_{2-x}(PO_4)_3$ ($M = Sc^{3+}$ or Y^{3+}) and their zirconium analogues," *J. Mater. Sci. Lett.,* **11** [12] 888-890 (1992).

[37]A. K. Ivanov-Schitz and J. Schoonman, "Electrical and interfacial properties of a $Li_3Fe_2(PO_4)_3$ single crystal with silver electrodes," *Solid State Ionics,* **91** [1-2] 93-99 (1996).

[38]C. R. Mariappan, M. Gellert, C. Yada, F. Rosciano, and B. Roling, "Grain boundary resistance of fast lithium ion conductors: Comparison between a lithium-ion conductive Li-Al-Ti-P-O-type glass ceramic and a $Li_{1.5}A_{10.5}Ge_{1.5}P_3O_{12}$ ceramic," *Electrochem. Commun.,* **14** [1] 25-28 (2012).

[39]C. Peters, A. Weber, B. Butz, D. Gerthsen, and E. Ivers-Tiffee, "Grain-Size Effects in YSZ Thin-Film Electrolytes," *J. Am. Ceram. Soc.,* **92** [9] 2017-2024 (2009).

[40]J. Wolfenstine, E. Rangasamy, J. L. Allen, and J. Sakamoto, "High conductivity of dense tetragonal $Li_7La_3Zr_2O_{12}$," *J. Power Sources,* **208** 193-196 (2012).

[41]N. Bonanos, B. C. H. Steele, and E. P. Bulter, "Characterization of Materials," pp. 205-264. in Impedance Spectroscopy: Theory, Experiment, and Applications 2nd Edition**.** Edited by E. Barsoukov and J. R. Macdonald. John Wiley & Sons, Inc, Hoboken, New Jersey, 2005.

[42]H. N. Al-Shareef, D. Dimos, B. A. Tuttle, and M. V. Raymond, "Metallization schemes for dielectric thin film capacitors," *J. Mater. Res.,* **12** [2] 347-354 (1997).

[43]C. T. Shelton, P. G. Kotula, G. L. Brennecka, P. G. Lam, K. E. Meyer, J.-P. Maria, B. J. Gibbons, and J. F. Ihlefeld, "Chemically homogeneous complex oxide thin films via improved substrate metallization," *Adv. Funct. Mater.,* **22** 2295-2302 (2012).

[44]L. Elammari, J. Durand, L. Cot, and B. Elouadi, "The structure of $NaZnPO_4$," *Z. Kristallogr.,* **180** 137-140 (1987).

[45]H. Okamoto, "Na-Pt (Sodium-Platinum)," pp. 2725-2726. in Binary Alloy Phase Diagrams*,* **Vol. 3.** Edited by T. B. Massalski. ASM International, Materials Park, OH, USA, 1990.

Figure Captions:

Figure 1: X-ray diffraction patterns for $Na_{1+x}Zr_2Si_xP_{3-x}O_{12}$ thin films prepared on platinized silicon substrates at temperatures of 750, 775, and 800 °C. Panels (a), (b), (c), and (d) correspond to patterns for compositions of x=0.25, x=0.50, x=0.75, and x=1.0, respectively. The black and gray bar markers indicate the positions of the x=0 NaSICon[20] and tetragonal ZrO_2[21] reflections, respectively.

Figure 2: Average crystal coherence length (crystallite size) of NaSICon thin films as a function of composition and processing temperature as determined from X-ray scattering data. The 800 °C data point for the x=1.0 composition is obscured by the 775 °C data point for the same composition.

Figure 3: Plan-view scanning electron micrographs of 800 °C processed NaSICon films of compositions (a) x=0.25, (b) x=0.50, (c) x=0.75, and (d) x=1.0. Levels and gamma adjustments were applied to enhance contrast using Adobe Photoshop.

Figure 4: Representative complex plane impedance spectra for $Na_{1+x}Zr_2Si_xP_{3-x}O_{12}$ thin films with platinum contacts processed at 800 °C for compositions (a) x=0.25, (b) x=0.50, and (c) x=0.75 and (d) x=1.0. The circuit diagram shown in (a) was used to fit all data. Open circles represent the raw measured data and the solid lines represent the modeled response. χ^2 values of 0.035, 0.865, 0.029, and 0.042 Ohms for the respective data ((a)-(d)) shown were calculated from the fits to the measured data.

Figure 5: Room temperature ionic conductivities of $Na_{1+x}Zr_2Si_xP_{3-x}O_{12}$ thin films as a function of processing temperature and composition. The data represent the average ion conductivity of three different electrodes on each sample and the error bars are the standard deviation. x=0 data is adapted from Meier, *et al.*[7]

Figure 6: Arrhenius plot of the sodium-ion conductivity of $Na_{1+x}Zr_2Si_xP_{3-x}O_{12}$ thin films processed at 800 °C and measured between ~21 °C and 150 °C for compositions of x=0.25 to x=1.0. Activation energies of 0.31 to 0.41 eV are calculated from the linear fit.

Figure 1:

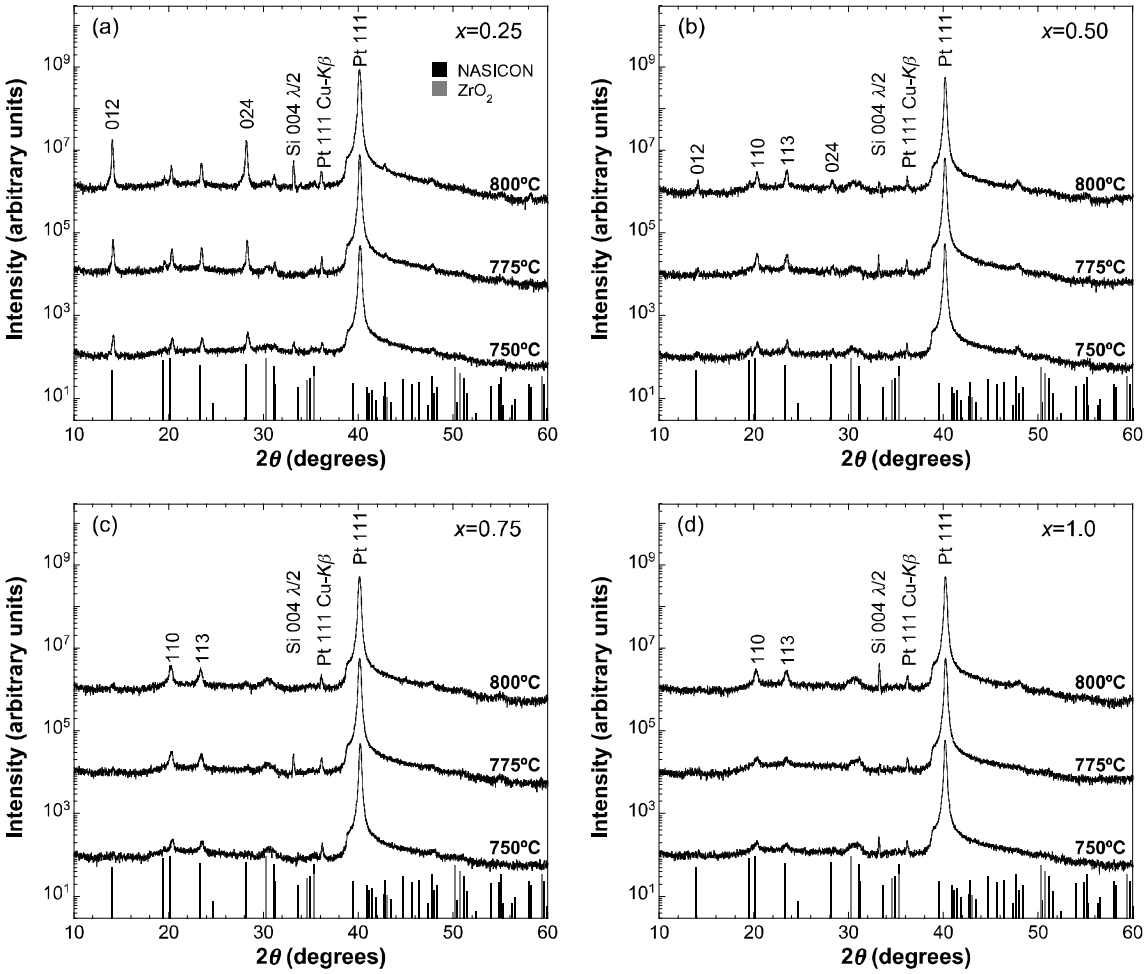

Figure 1: X-ray diffraction patterns for $Na_{1+x}Zr_2Si_xP_{3-x}O_{12}$ thin films prepared on platinized silicon substrates at temperatures of 750, 775, and 800 °C. Panels (a), (b), (c), and (d) correspond to patterns for compositions of x=0.25, x=0.50, x=0.75, and x=1.0, respectively. The black and gray bar markers indicate the positions of the x=0 NaSICon[19] and tetragonal ZrO_2[20] reflections, respectively.

Figure 2:

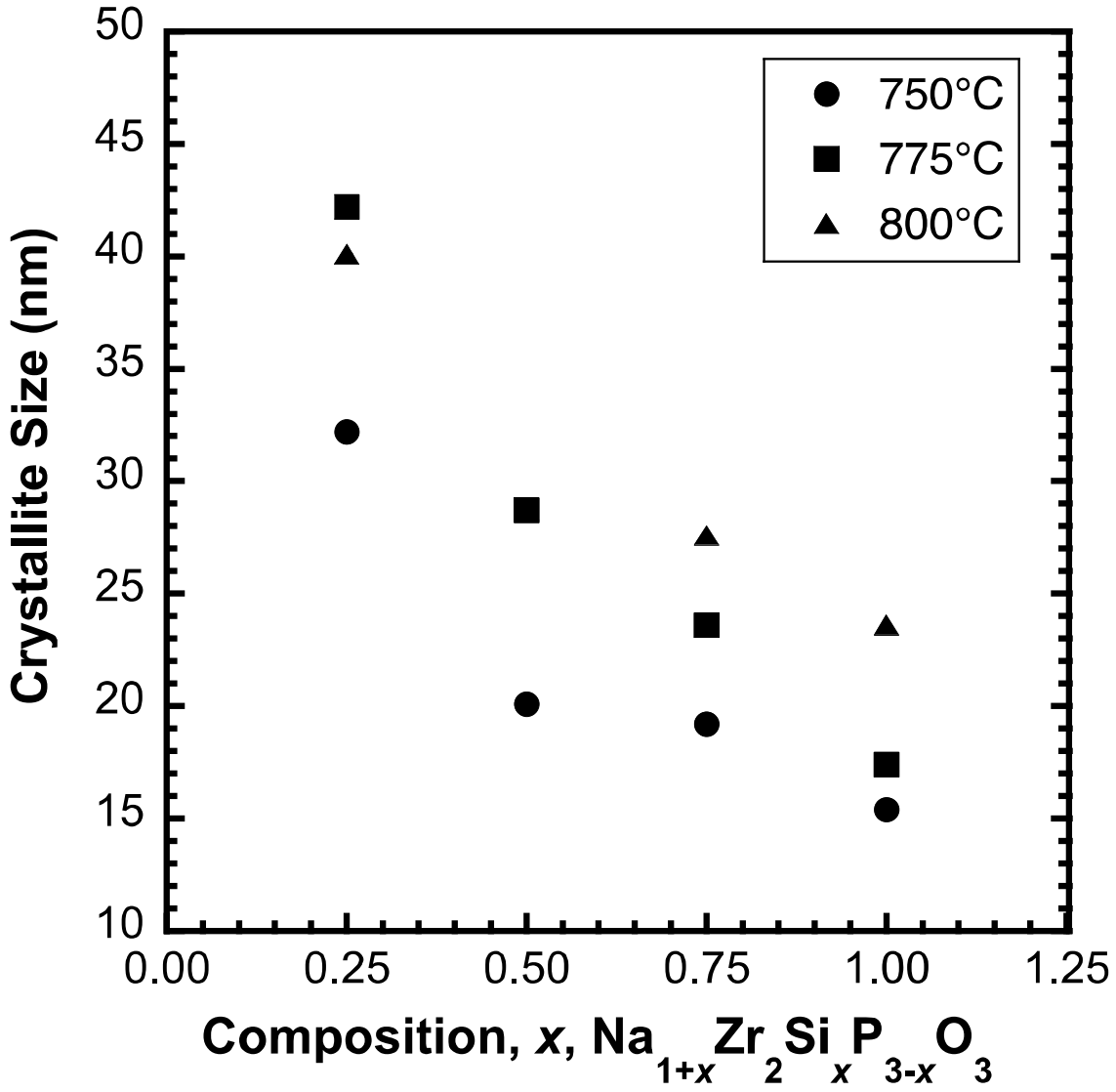

Figure 2: Average crystal coherence length (crystallite size) of NaSICon thin films as a function of composition and processing temperature as determined from X-ray scattering data. The 800 °C data point for the x=0.5 composition is obscured by the 775 °C data point for the same composition.

Figure 3:

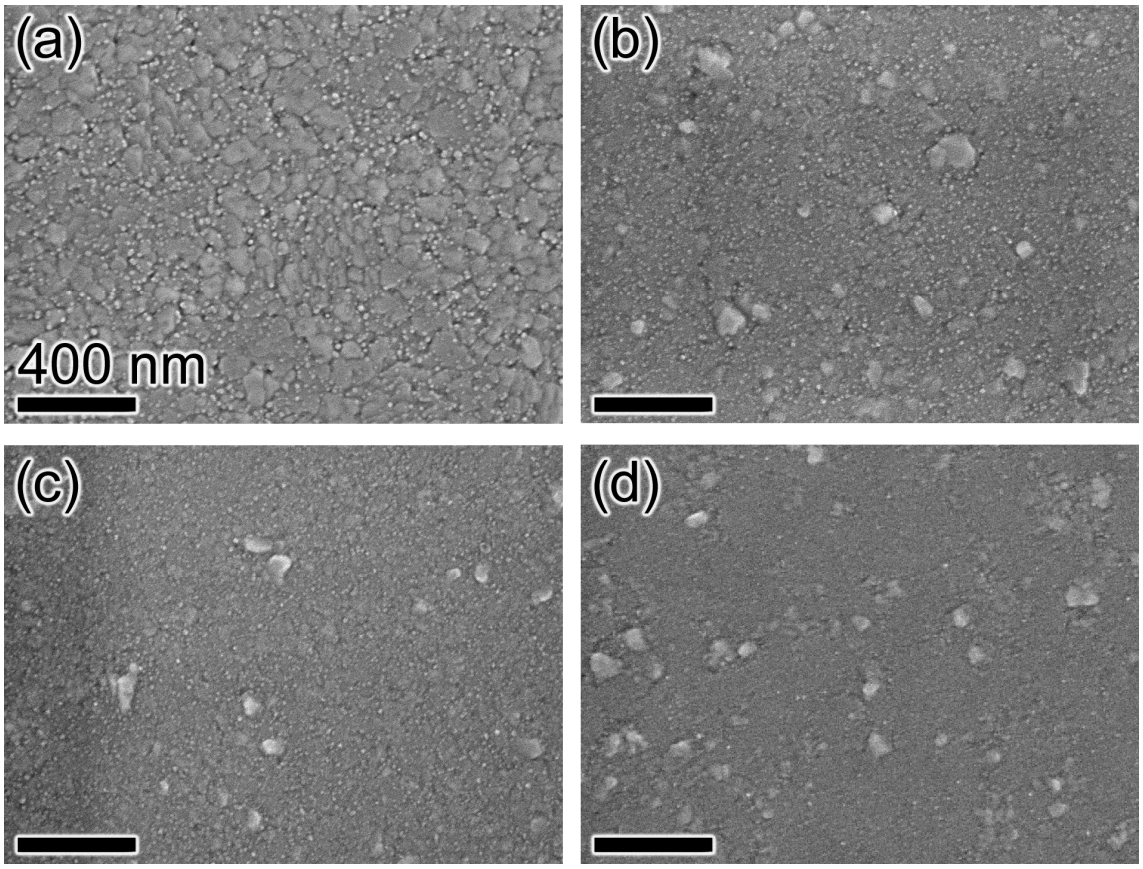

Figure 3: Plan-view scanning electron micrographs of 800 °C processed NaSICon films of compositions (a) x=0.25, (b) x=0.50, (c) x=0.75, and (d) x=1.0.

Figure 4:

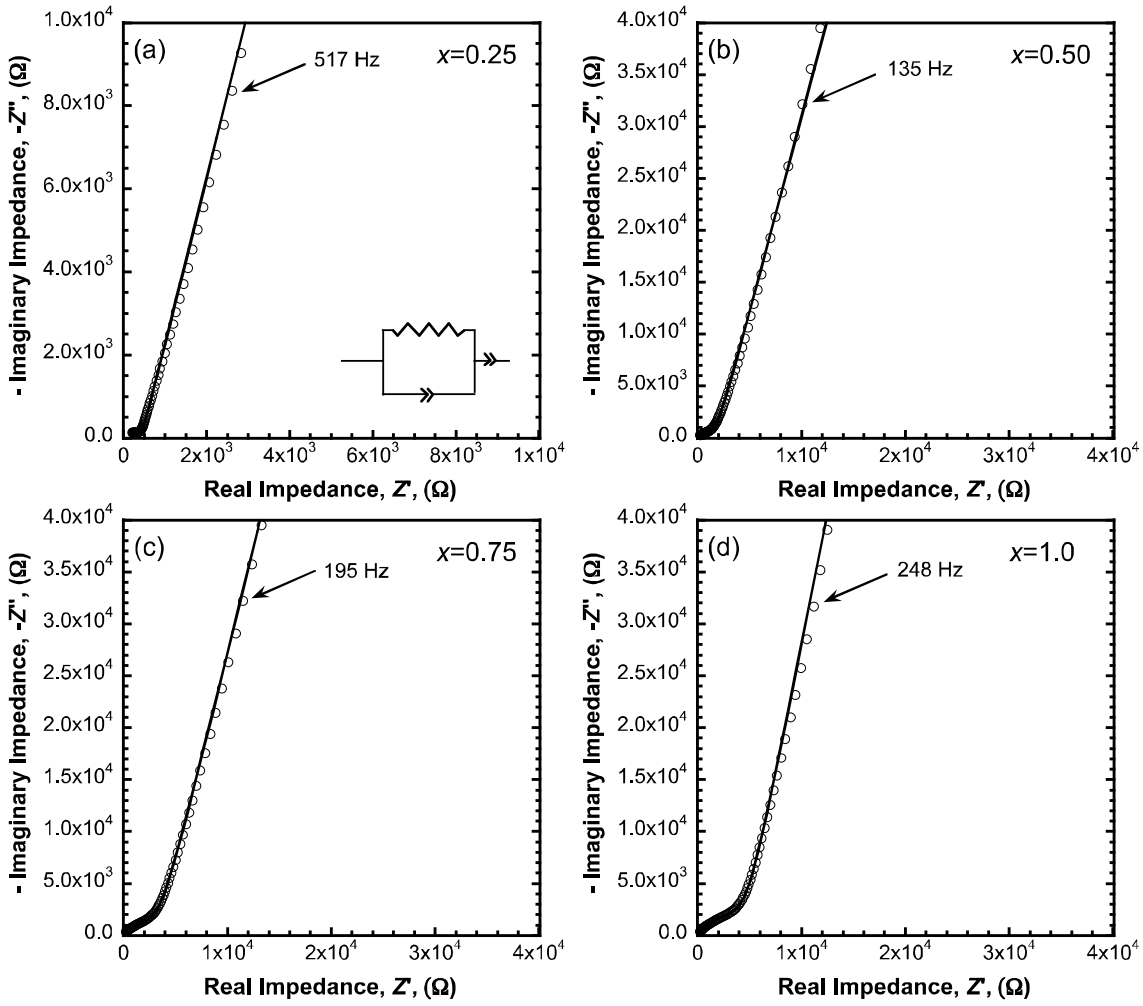

Figure 4: Representative complex plane impedance spectra for $Na_{1+x}Zr_2Si_xP_{3-x}O_{12}$ thin films with platinum contacts processed at 800 °C for compositions (a) x=0.25, (b) x=0.50, and (c) x=0.75 and (d) x=1.0. The circuit diagram shown in (a) was used to fit all data. Open circles represent the raw measured data and the solid lines represent the modeled response. χ^2 values of 0.035, 0.865, 0.029, and 0.042 Ohms for the respective data ((a)-(d)) shown were calculated from the fits to the measured data.

Figure 5:

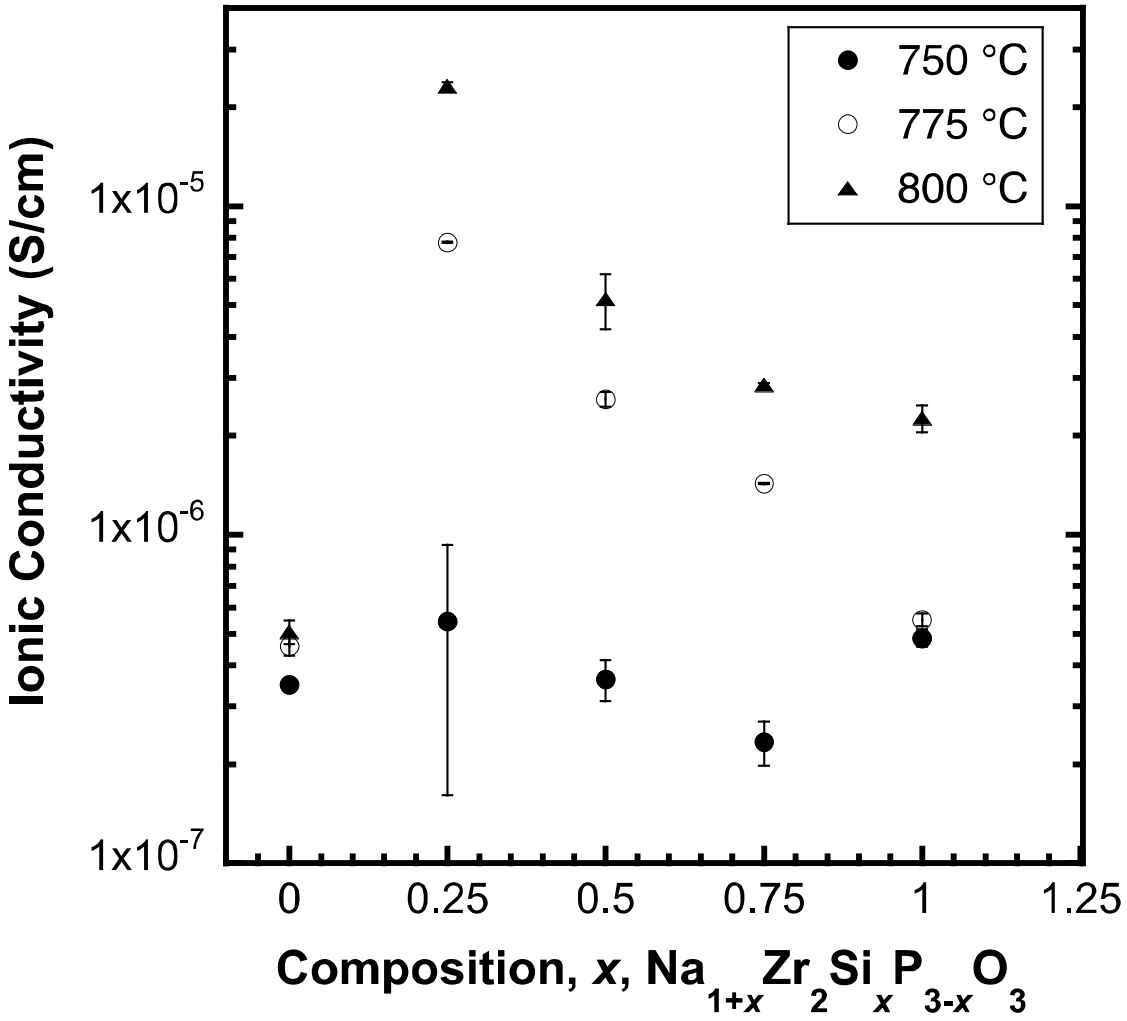

Figure 5: Room temperature ionic conductivities of $Na_{1+x}Zr_2Si_xP_{3-x}O_{12}$ thin films as a function of processing temperature and composition. The data represent the average ion conductivity of three different electrodes on each sample and the error bars are the standard deviation. x=0 data is adapted from Meier, *et al.*[7]

Figure 6:

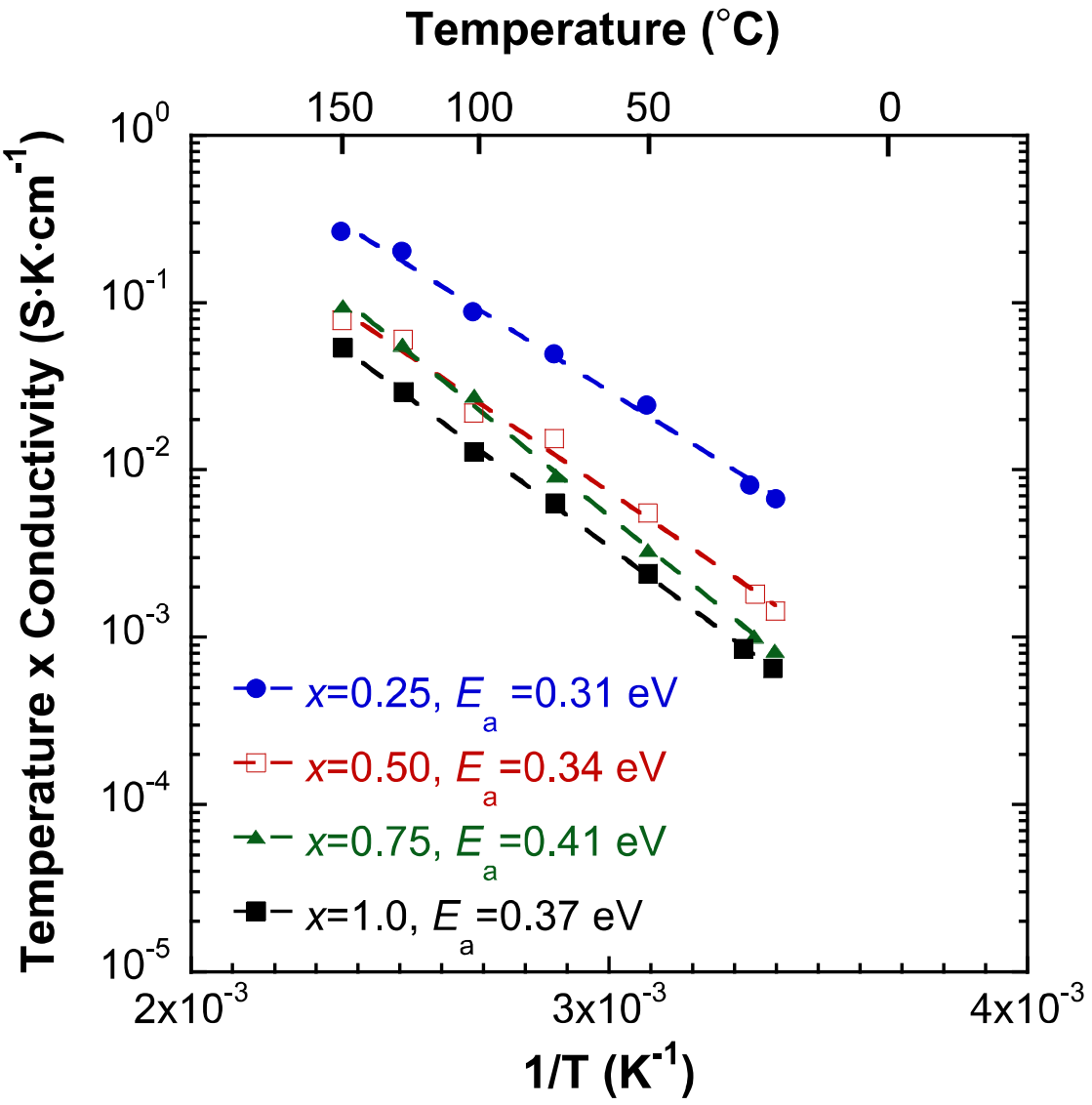

Figure 6: Arrhenius plot of the sodium-ion conductivity of $Na_{1+x}Zr_2Si_xP_{3-x}O_{12}$ thin films processed at 800 °C and measured between ~21 °C and 150 °C for compositions of x=0.25 to x=1.0. Activation energies of 0.31 to 0.41 eV are calculated from the linear fit.

Silicon incorporation and scaling effects in sodium zirconium silicate phosphate ($Na_{1+x}Zr_2Si_xP_{3-x}O_{12}$) ion conducting thin films

Jon F. Ihlefeld[1, a), *] Emily Gurniak,[1] Brad H. Jones,[1] David R. Wheeler,[1] Mark A. Rodriguez,[1] and Anthony H. McDaniel[2, *]

[1]*Sandia National Laboratories, Albuquerque, New Mexico 87185, USA*
[2]*Sandia National Laboratories, Livermore, California, 94551 USA*

Supplemental Information:

a) Electronic mail: jihlefe@sandia.gov
* Member, The American Ceramic Society

Figure S1:

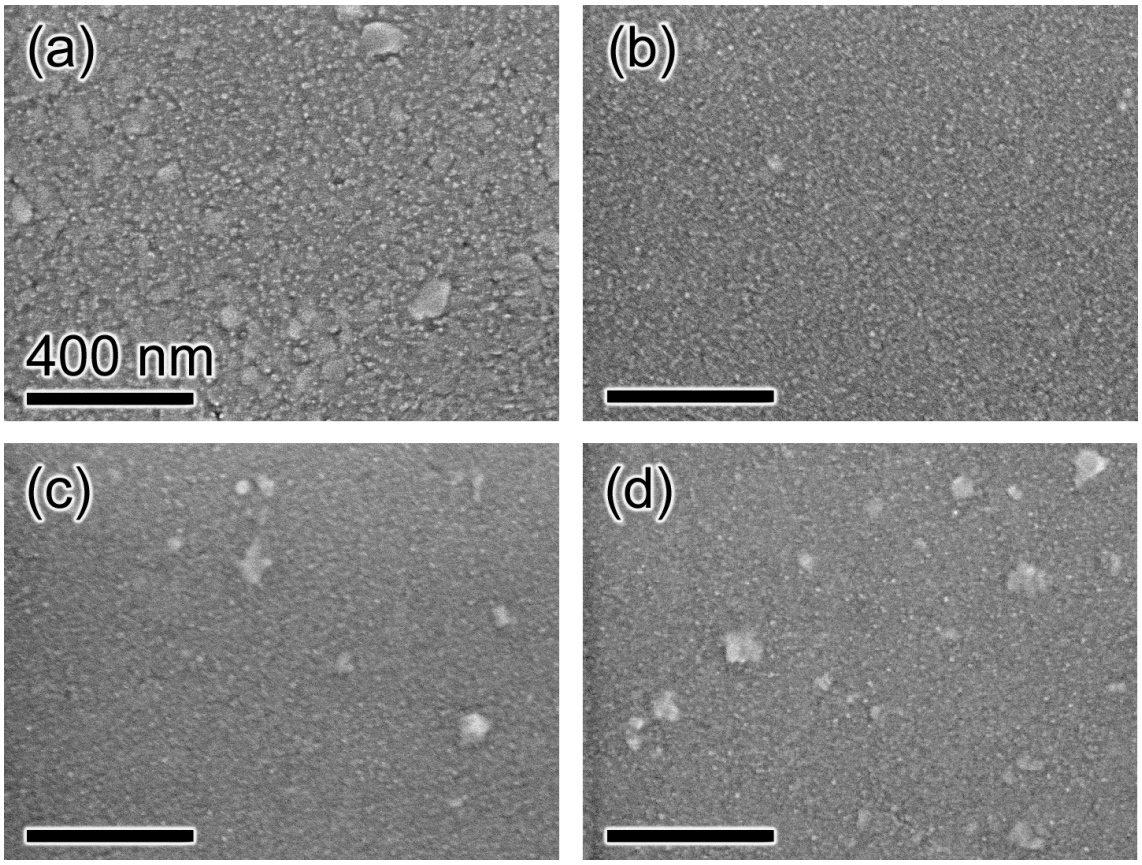

Figure S1: Plan-view scanning electron micrographs of 750 °C processed NaSICon films of compositions (a) x=0.25, (b) x=0.50, (c) x=0.75, and (d) x=1.0.

Figure S2:

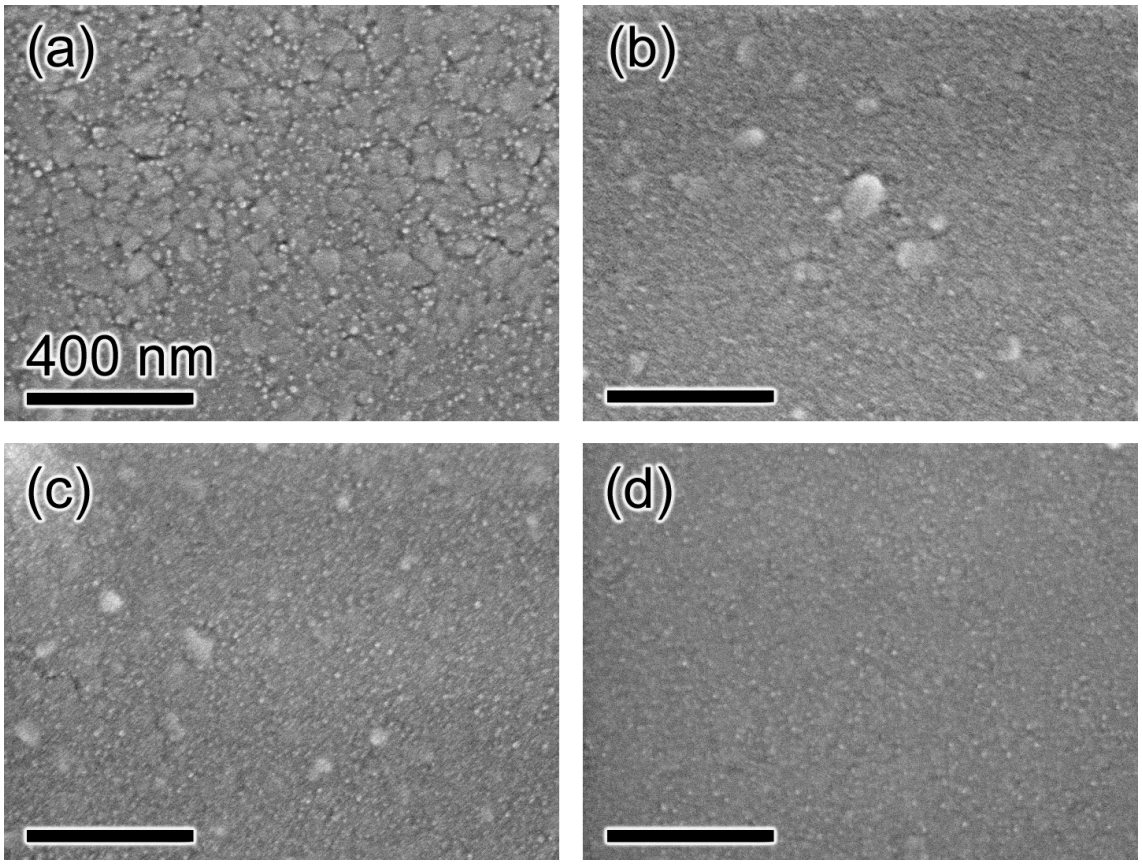

Figure S2: Plan-view scanning electron micrographs of 775 °C processed NaSICon films of compositions (a) x=0.25, (b) x=0.50, (c) x=0.75, and (d) x=1.0.

Figure S3:

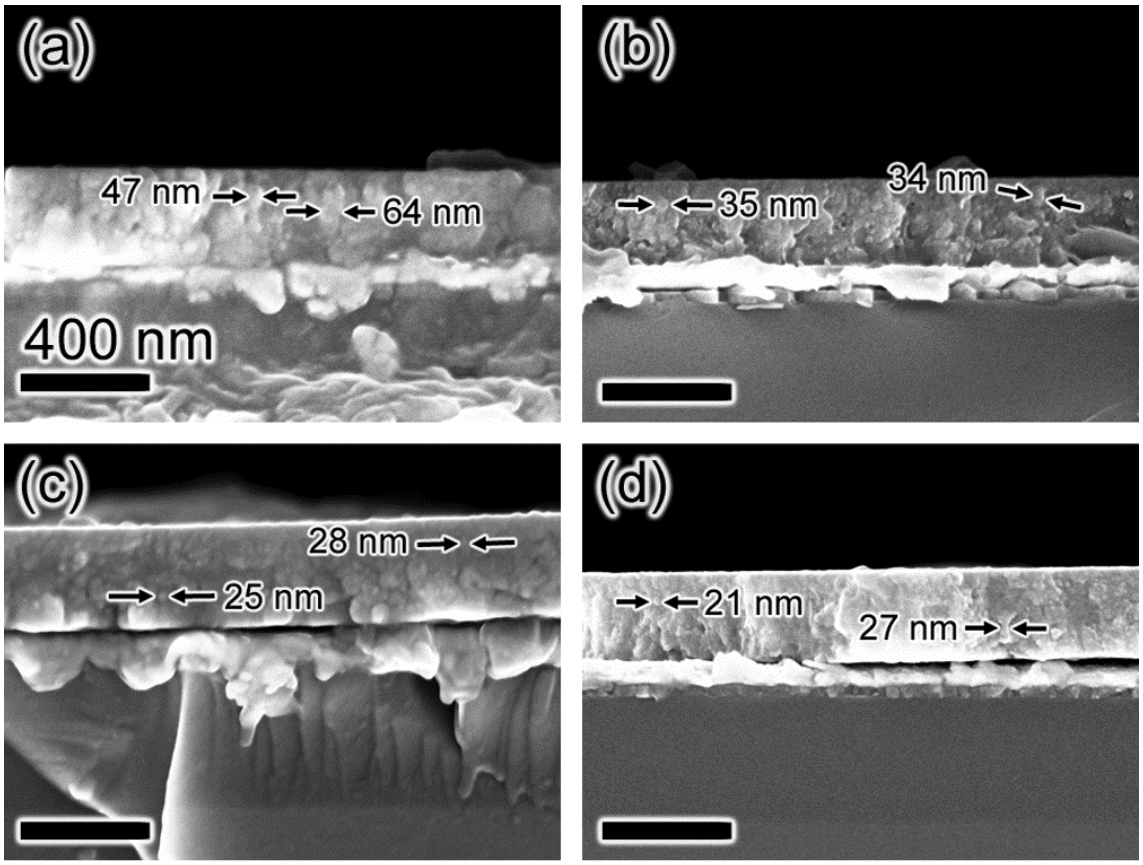

Figure S3: Cross-sectional SEM images of (a) x=0.25, (b) x=0.50, (c) x=0.75, and (d) x=1.0 NaSICon films processed at 750 °C. Granular features and their dimensions are noted on the micrographs.

Figure S4:

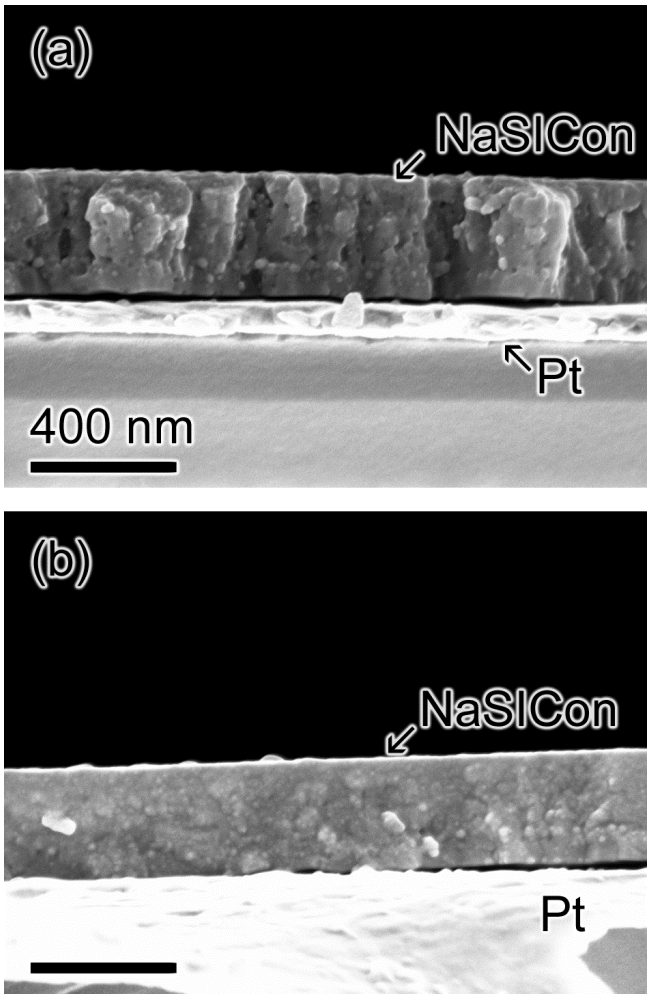

Figure S4: Cross-sectional SEM images of (a) x=0.25 NaSICon and (b) x=0.75 NaSICon films processed at 800 °C.

Table SI: Complex plane impedance fit parameters for representative 800 °C processed x=1 composition NASICON film using a R1+Q1/R2+Q2 equivalent circuit.

Element	Value
Resistor, R, 1	3.206×10^{-6} Ohms
Constant Phase Element, Q, 1	0.1016×10^{-6} F•s$^{1/a}$
Constant Phase Element, α, 1	0.6367
Resistor, R, 2	4761 Ohms
Constant Phase Element, Q, 2	48.46×10^{-9} F•s$^{1/a}$
Constant Phase Element, α, 2	0.8779

Table SII: Complex plane impedance fit parameters for the same 800 °C processed x=1 composition NASICON film as in Table SI using a R1+Q1/R2+Q2/R3+Q3 equivalent circuit. Note that R3 has a value of 10^{-18} Ohms indicating a lack of improvement of fit by including the additional ZARC (Q2/R3) element.

Element	Value
Resistor, R, 1	0.7973×10^{-12} Ohms
Constant Phase Element, Q, 1	0.1016×10^{-6} F•s$^{1/a}$
Constant Phase Element, α, 1	0.6367
Resistor, R, 2	4761 Ohms
Constant Phase Element, Q, 2	6.86×10^{36} F•s$^{1/a}$
Constant Phase Element, α, 2	0.9969
Resistor, R, 3	0.3525×10^{-18} Ohms
Constant Phase Element, Q, 3	48.46×10^{-9} F•s$^{1/a}$
Constant Phase Element, α, 3	0.8779

Figure S5:

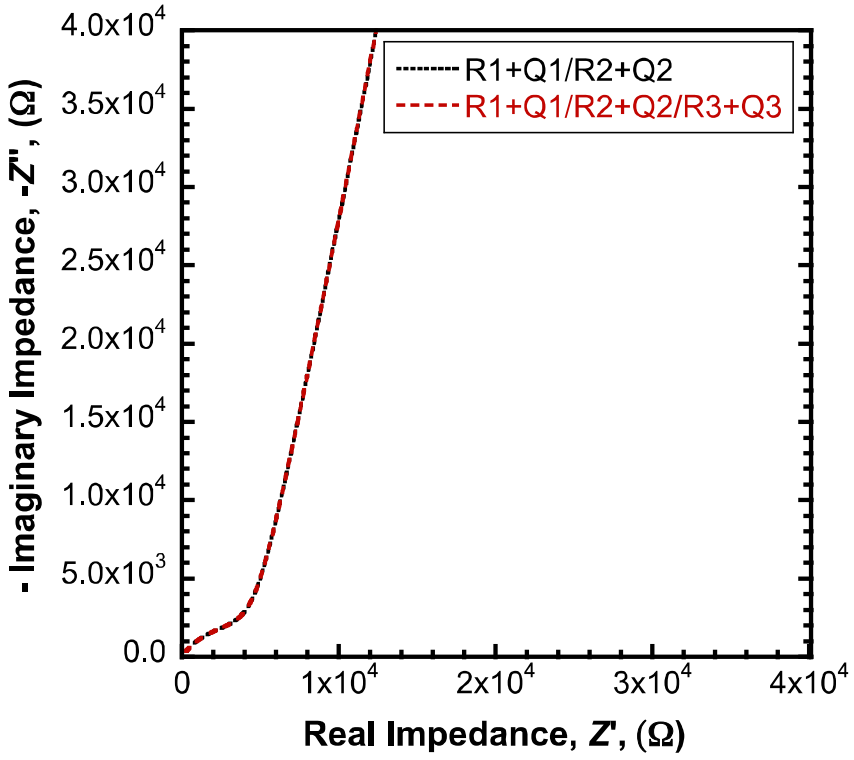

Figure S5: Comparison of the impedance models from Tables S1 (R1+Q1/R2+Q2 data) and SII (R1+Q1/R2+Q2/R3+Q3 data) for an 800 °C processed *x*=1 NaSICon film. These models were fit to the same data as shown in Figure 4d.

Figure S6:

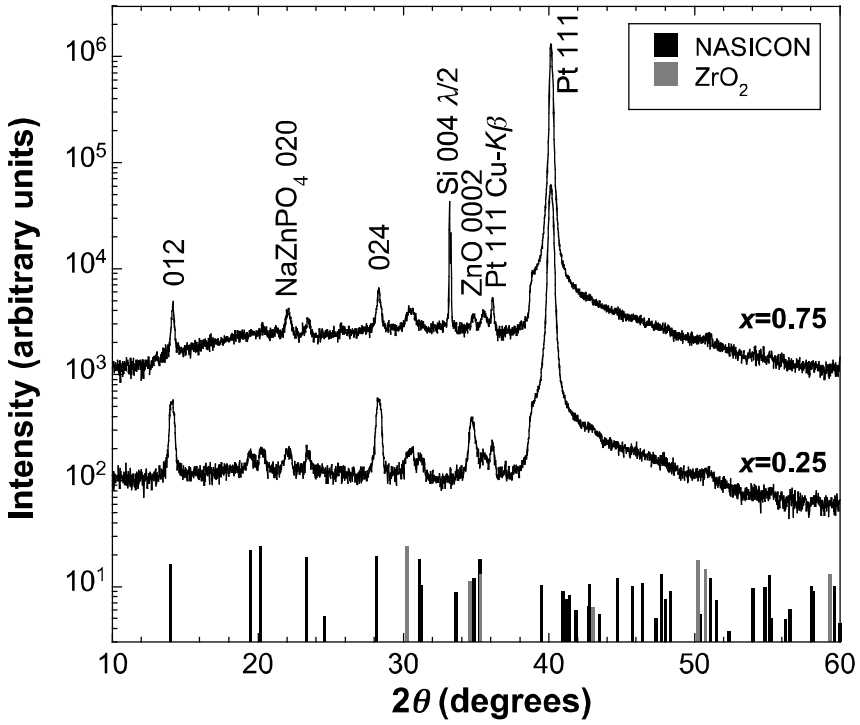

Figure S6: X-ray diffraction patterns of x=0.25 and x=0.75 NaSICon processed on Pt/ZnO/SiO_2/Si substrates at 800 °C. A secondary phase of $NaZnPO_4$ is observed in both films.

Figure S7:

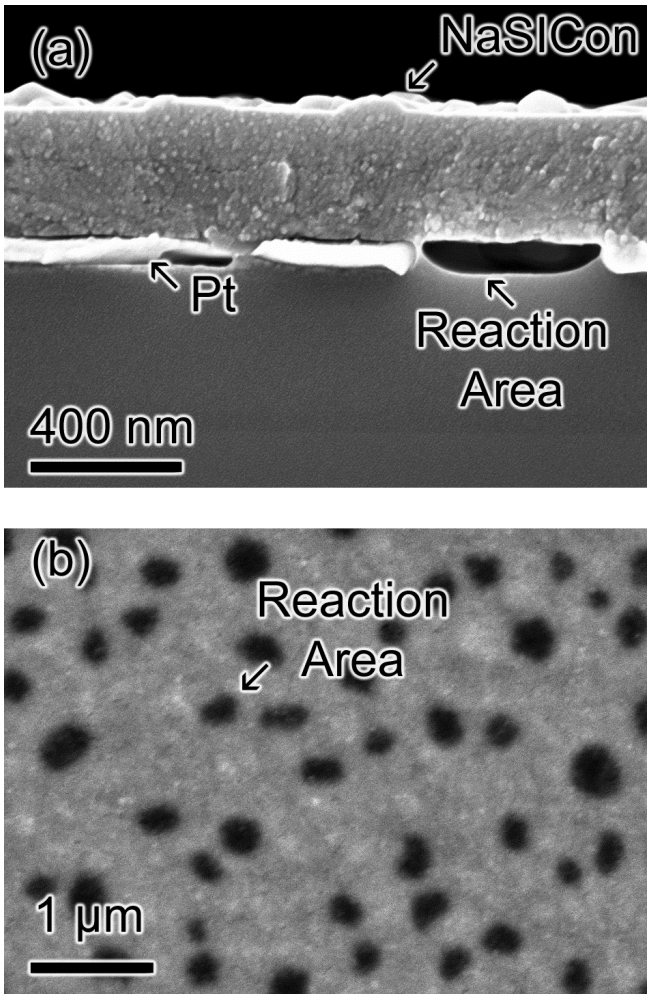

Figure S7: (a) Cross-sectional in-lens SEM image of an x=1 NaSICon film prepared on a Pt/ZnO/SiO_2/Si substrate at 750 °C. Dewetting of the platinum layer is evident and labeled as the reaction layer. (b) Secondary electron SEM image collected with a 15 kV accelerating voltage of an x=1 NaSICon film prepared on a Pt/ZnO/SiO_2/Si substrate at 800 °C. This high accelerating voltage allows for a substantial electron interaction volume and imaging of the platinum film. The reaction areas in the image are holes in the platinum layer.